ELSEVIER

www.elsevier.nl/locate/jorganchem

Journal of Organometallic Chemistry 599 (2000) 42–48

Journal of Organometallic Chemistry

Langmuir–Blodgett films of the endohedral metallofullerene $Dy@C_{82}$ at the air–water interface

Houjin Huang, Shihe Yang *

Department of Chemistry, Hong Kong University of Science and Technology, Clear Water Bay, Kowloon, Hong Kong, PR China

Abstract

Multilayer Langmuir–Blodgett (LB) films of the endohedral metallofullerene $Dy@C_{82}$ were constructed for the first time at the air–water interface. High-resolution transmission electron microscopy of these films revealed short-range ordered metallofullerene assemblies as well as layered structures. Individual metallofullerenes appeared intact after being transferred from the air–water interface. Blue-shifted UV–vis absorption peaks were observed and attributed to the partial oxidation of the metallofullerene balls. © 2000 Elsevier Science S.A. All rights reserved.

Keywords: Langmuir–Blodgett film; Endohedral metallofullerene

1. Introduction

Soon after the discovery of the synthetic route for macroscopic production of C_{60} and C_{70}, the Langmuir–Blodgett (LB) technique was applied to prepare C_{60} and C_{70} films at the air–water interface [1–7]. It was found that only multilayers were formed at the air–water interface for all these carbon molecules. In recent years, C_{60} ex-derivatives have also been explored as LB film materials [8–10]. By controlling the amphiphilicity of the derivatized fullerenes, high-quality LB films could be prepared at the layer-by-layer level. To our knowledge, however, no fabrication of LB films of endohedral metallofullerenes has been reported. This may be due partly to the difficulties in obtaining a sufficient amount of pure metallofullerene samples and to doubts about their stability at the air–water interface. Clearly, investigations of LB assemblies of endohedral metallofullerenes are important not only for understanding the inter-metallofullerene interactions, but also for development of potential devices [11]. Here, we report for the first time the preparation of LB films of the endohedral metallofullerene $Dy@C_{82}$ at the air–water interface. In a way similar to C_{60}, a multi-layer LB film was obtained and is attributed to the strong inter-metallofullerene interactions. Well-ordered structures were clearly observed by high-resolution transmission electron microscopy (TEM), indicating that the metallofullerene cages could survive the conditions at the water–air interface. Blue-shifted UV–vis absorption peaks were observed and attributed to the partial oxidation of the metallofullerenes.

2. Experimental

As described previously, high-purity metallofullerene $Dy@C_{82}$ ($>99.0\%$) was obtained by the standard arc-discharge method [12–14]. The raw soot was subjected to Soxhlet extraction using DMF as a solvent, followed by HPLC separation using a 5PYE column and a mobile phase of toluene. The collected $Dy@C_{82}$ toluene solution was concentrated and re-purified with the same HPLC column just before use for spreading onto the water surface. The identity and purity of the sample was verified by methane DCI negative-ion mass spectrometry.

For LB film preparation, freshly distilled ultrapure water (through an ultrapure water system) was used as the sub-phase. Before spreading, the water surface was cleaned using a 100 ml syringe to ensure that the maximum surface pressure difference was less than 0.2 mN m^{-1} upon compression. The initial concentration of the metallofullerene solution (2.05×10^{-5} M) was determined by weighing a vacuum-dried solid in a

* Corresponding author. Fax: +852-2358-9180.
E-mail address: chsyang@ust.hk (S. Yang)

0022-328X/00/$ - see front matter
PII: S0022-328X(99)00712-3

known volume of solution using a precision balance (Autobalance model AD-6). In each run of experiments, a known volume (1–10 ml) of the metallofullerene solution was carefully dropped onto the water surface (554 cm^2) using a 1 ml syringe. After the solvent evaporated completely ($\sim$30 min), the barrier was compressed slowly ($\sim$1 cm min^{-1}). No significant difference in the resulting isotherms was observed with different compression speeds.

The metallofullerene films formed at the air–water interface were transferred onto fused quartz plates using the vertical transfer method for UV–vis absorption spectroscopy. The surface pressure was kept at 20 mN m^{-1} during the transfer. UV–vis absorption spectra were recorded with a Milton Roy spectrometer (Spectronic 3000). High-resolution TEM was carried out using a Jeol 2010 TEM operated at 200 kV. For TEM examination, a holey carbon film on a copper grid was immersed under the water surface and then lifted slowly until the floating metallofullerene film was deposited on the grid. The surface pressure was also kept at 20 mN m^{-1}.

3. Results and discussion

Fig. 1(a) shows an HPLC trace of the crude extract of fullerenes and Dy-containing metallofullerenes redissolved in toluene after evaporation of DMF. A prominent peak appears at $\sim$24.0 min, which is absent for samples produced from arc-discharge of a pure carbon electrode. This peak is apparently from Dy@C_{82}, as identified by the negative-ion mass spectrum shown in Fig. 2. Because the peak of Dy@C_{82} is somewhat overlapped with that of C_{88} right after it, we collected only the eluate fraction before the C_{88} shoulder. Fig. 1(b) shows an HPLC profile of the collected fraction of Dy@C_{82} in Fig. 1(a). The HPLC profile of the purified sample shows a single clean peak due to Dy@C_{82}. The mass spectrum corresponding to this clean peak is displayed in Fig. 2. As shown in Fig. 2, the observed isotope distribution is consistent with the expected isotope distribution for Dy@C_{82}. The intensities of empty fullerenes are significantly smaller than that of Dy@C_{82}, and the purity of our sample is estimated to be $\sim$95%.

The π–A isotherm of the endohedral metallofullerene Dy@C_{82} on the pure water surface is shown in Fig. 2. This is the third compression–expansion cycle, and the two pre-compression cycles were reversed at a lower surface pressure ($<$20 mN m^{-1}). The most striking feature of this π–A isotherm is the presence of a large hysteresis loop even after two pre-compression cycles, suggesting strong attractive interactions between metallofullerene particles. The LB film at the air–water interface appeared remarkably rigid and visibly patchy while reversing the barrier. The compression could be continued until $\sim$40 mN m^{-1}, above which the LB film collapsed and some hair-like black crevices of $\sim$1 cm long were observed on the water surface. The limiting 'area per molecule' is estimated to be $\sim$36 $Å^2$ from the third compression process. This value is obviously smaller than the minimum cross section of such molecules (e.g. $\sim$120 $Å^2$ for Y@C_{82} based on an X-ray diffraction study [15]), but still significantly larger than that of C_{60} estimated from its LB π-A isotherm ($<$28 $Å^2$ $molecule^{-1}$ [2–7]). After all, the diameter of C_{82} is surely somewhat larger than that of C_{60}.

Although a multilayer LB film of C_{60} was obtained in most cases, careful control of such experimental conditions as concentration ($<10^{-4}$ M) could lead to the formation of monolayer LB film of C_{60} at the air–water interface [1,6]. As for the endohedral metallofullerene Dy@C_{82}, however, only multilayer films (3–6 layers estimated from the π–A isotherms) are formed even at a very low concentration ($<10^{-5}$ M). This is demonstrated in the inset of Fig. 2, in which the estimated limiting 'molecular area' of Dy@C_{82} is shown to be only slightly larger at lower concentration, but still far below the true value. A further contrast is that the π–A isotherm of Dy@C_{82} is not as steep ($\sim$3.12 mN molecule $Å^{-2}$) as that of C_{60} ($>$10 mN molecule $Å^{-2}$), indicating a poorer arrangement of the metallofullerene molecules than that of C_{60}. Apparently, C_{60} and Dy@C_{82} are quite different in the sense that C_{60} is highly symmetric while Dy@C_{82} is known to have a dipole moment, and a stronger interaction between the metallofullerenes is expected.

A typical high-resolution TEM micrograph is shown in Fig. 3. First of all, layered structures can be identified based on the TEM image. The different image contrast at the layer edges indicates the presence of 3–6 layers, a result which is consistent with that based on the π–A isotherm shown in Fig. 2. It is remarkable that individual metallofullerene balls can also be clearly recognized with a shortest inter-metallofullerene distance of $\sim$1.0 nm. Evidently, the integrity of the metallofullerene molecules was preserved after transfer from the air–water interface. It should be pointed out that although the metallofullerene cages can survive the conditions at the air–water interface, EDX (energy-dispersive X-ray fluorescence) showed the presence of not only C and Dy elements, but also O in the sample (not shown here), indicating oxidation. This was also shown in the XPS data, which will be described below. Finally, the TEM image shows a short-range ordered structure within the layers; the fringe spacing is $\sim$1.05 nm, which is close to the size of the metallofullerene. It was found that overlapping the same TEM image, but rotating it by a small angle, would produce concentric circles ('Moiré ring' pattern), which change with the angle of rotation. This demonstrates that the metallo-

fullerene assembly has indeed certain peculiar ordered structures, which are perhaps dictated by the balance between the ball nature of the metallofullerene, its intrinsic dipole moment and the oxygen substituents on the metallofullerene surface. In the inset of Fig. 3, an electron diffraction pattern of the metallofullerene LB film is shown. The first-order diffraction pattern has a slightly deformed hexagonal shape with two brightest diffraction spots at two opposing corners. These two diffraction spots correspond to a d-spacing of ~ 0.98 nm, which is close to the fringe spacing estimated above from the real space HRTEM image. The higher brightness of the two diffraction spots suggests that the metallofullerene packing in this particular direction has a higher degree of order.

Fig. 4 shows an XPS pattern of the Dy@C_{82} LB film (Fig. 4(a)) along with that of its counterpart $DyCl_3$ (Fig. 4(b)) in the core-level region of Dy 4d. First of all, the XPS profile of the LB film verifies the successful transfer of the metallofullerenes from the air–water

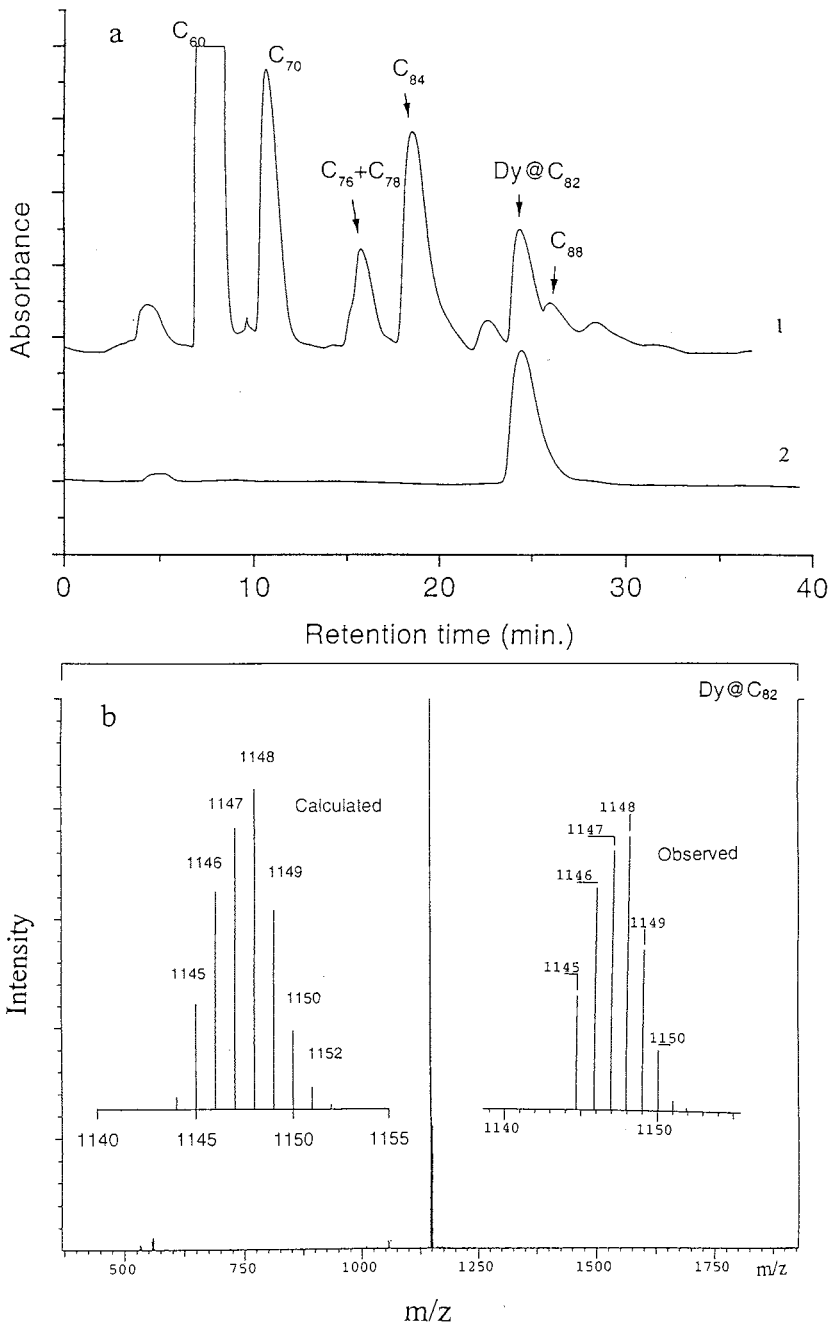

Fig. 1. (a) HPLC chromatograms of a crude Dy@fullerene extract redissolved in toluene (trace 1), and a purified Dy@C_{82} sample (trace 2); (b) DCI methane negative-ion mass spectrum of a purified Dy@C_{82} sample. The inset shows the observed and calculated isotope distributions of Dy@C_{82}.

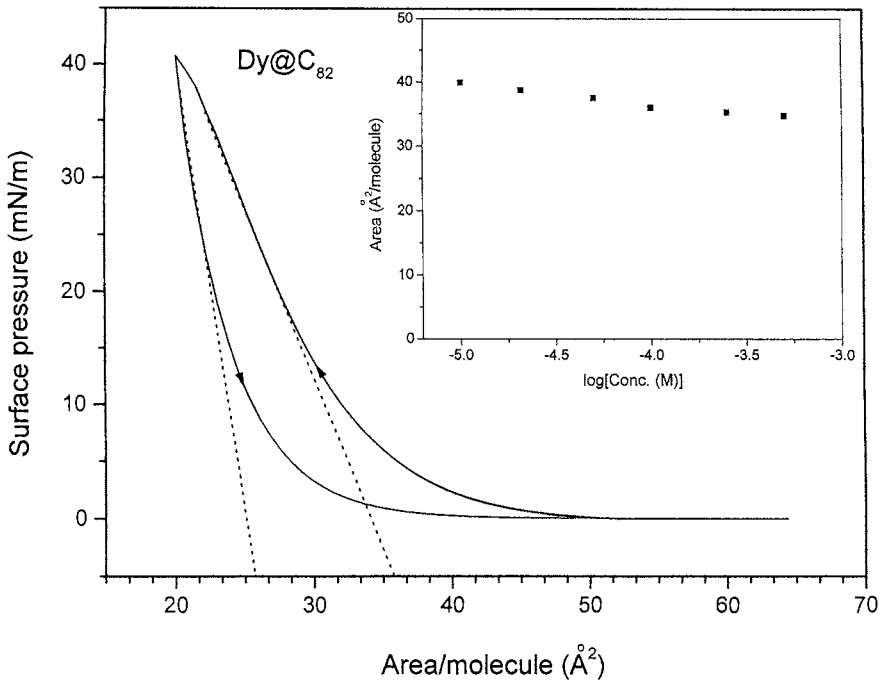

Fig. 2. π–A isotherm of Dy@C_{82} at a compression–expansion speed of $\sim$1 cm min^{-1}, after two cycles reversed at 20 mN m^{-1}. The inset shows the dependence of the concentration of Dy@C_{82} on the limiting 'area per molecule'.

interface. Second, the comparison of the XPS patterns of these two compounds shows a striking similarity. Specifically, they all exhibit five peaks with similar peak separations and intensity distributions. For example, the peaks of Dy@C_{82} are found at 153.86, 155.39, 157.78, 159.87 and 163.58 eV, while the corresponding peaks of $DyCl_3$ are at 153.50, 155.52, 158.20, 160.26 and 163.20 eV. This shows that the Dy atom is still trapped inside the carbon cage. The reason is that if the carbon cage were broken, metal oxides would form, yielding a rather different XPS pattern from what we observed.

The XPS pattern of Dy@C_{82} LB film in the core-level region of C 1s is shown in Fig. 4(c). The two small shoulder peaks next to the main peak suggest the presence of oxygen bonded to carbon. A simple curve-fitting analysis shows that three peaks are required to fit the core-level (C 1s) features, implying the presence of two different carbon oxidation states in addition to the normal carbon oxidation state (non-oxygenated carbon) associated with the main peak. The peak at a binding energy of 285.0 eV (77.4%) is assigned to the non-oxygenated carbons, while the peak at a binding energy of 286.8 eV (14.0%) is assigned to the carbons linked to a single oxygen by a σ bond. Another peak is located at a binding energy of 288.6 eV (8.6%), which is nearly 3.6 eV higher than that of the main peak, suggesting the possible existence of dioxygenated or cyclooxygenated carbons. A rough estimate of the relative XPS peak intensities reveals that the metallofullerene sample contains $\sim$12 mono-oxygenated carbons and $\sim$7 dioxygenated carbons after spreading at the air–water interface. Although the oxygenated metallofullerenes are normally water soluble [16], multilayer LB films can still be formed at the air–water interface because the metallofullerenes were irreversibly linked together by the relatively strong dipole–dipole interactions before significant oxidation took place. Another possibility is that the oxygen atoms may act as a linkage between the metallofullerenes, which form a polymer network insoluble in water. It should be pointed out that the extent of oxidation presumably depends on the air exposure time. For this particular sample used in the XPS measurement, the air exposure time was relatively long (10 days) so that substantial oxidation has occurred to the metallofullerenes.

Fig. 5 shows the UV–vis spectra of Dy@C_{82} LB-films of different thickness. Since the transfer ratio ($\sim$0.2) was significantly smaller than unity, the number near each LB film spectrum actually represents the number of deposition steps instead of number of layers. For comparison, pure Dy@C_{82} in a toluene solution (0.0235 mg ml^{-1}) was recorded and is shown in the same figure. Several features are noteworthy. First, the LB film spectra are somewhat similar to the solution spectrum, but display peak shifts. As shown in the inset of Fig. 5, the peaks around 289 and 633 nm in the solution spectra are blue-shifted to 238 and 590 nm in the LB film spectra, respectively. The similarity between the LB spectra and the solution spectrum suggests that the integrity of the metallofullerenes upon film forma-

tion is indeed preserved and furthermore, oxidation of the metallofullerenes is not extensive. Note that for the UV–vis absorption measurement, care was taken to minimize the air exposure time of the metallofullerene film. Next, the absorption peaks of the LB film spectra are substantially broader than that of the corresponding solution spectrum. Perhaps due to this peak broadening, the shoulder peak around 400 nm becomes undetectable in the LB film. In addition, the absorption peak broadening becomes more severe with the increase of the film thickness.

The blue-shift of absorption peaks of the Dy@C_{82} film is in marked contrast to the red-shift in the absorption spectra of C_{60} films [2–7]. Since partial oxidation of the metallofullerenes is inevitable at the air–water interface, we tentatively attribute the blue-shifted spectral peaks to the oxygenated metallofullerenes. We believe that the metallofullerene sample used in the UV–vis measurement was only slightly oxygenated because otherwise the UV–vis spectrum of the metallofullerene film will be completely different from the pristine metallofullerenes.

We have also studied the LB film spreading behavior with both basic and acidic subphases. Fig. 6 shows π–A isotherms of Dy@C_{82} with subphases at pH $\approx$ 14 ([NaOH] = 0.063 mol l^{-1}) (Fig. 6(a)) and pH 1 ([HCl] = 0.090 mol l^{-1}) (Fig. 6(b)). In much the same way as for the case at pH 7 (Fig. 2), the isotherms were recorded at a compression–expansion speed of $\sim$1 cm min^{-1}. after two cycles reversed at a surface pressure of 20 mN m^{-1}. The second compression–expansion cycles in Fig. 6(a and b) were performed 1 h after their corresponding first cycles. Some differences are obvious at first sight between the isotherm curves recorded at

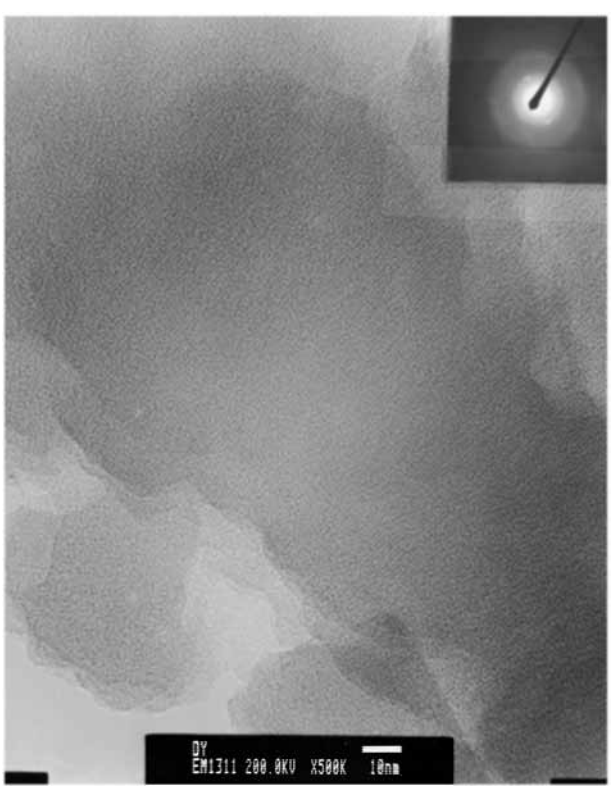

Fig. 3. High-resolution TEM image of Dy@C_{82} LB film deposited on a holey carbon film on a copper grid at a surface pressure of 20 mN m^{-1}. The inset shows the selected-area electron diffraction pattern.

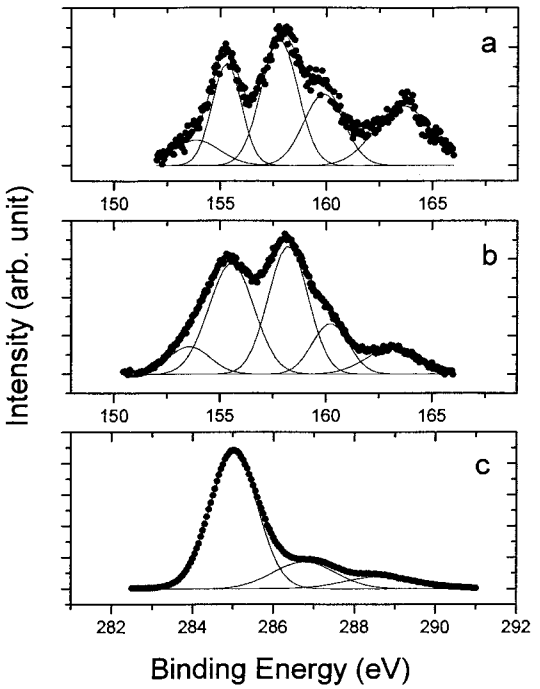

Fig. 4. XPS patterns of the Dy@C_{82} LB films (a) and $DyCl_3$ (b) in the core-level region of Dy 4d. (c) XPS pattern of the Dy@C_{82} LB films in the core-level region of C 1s.

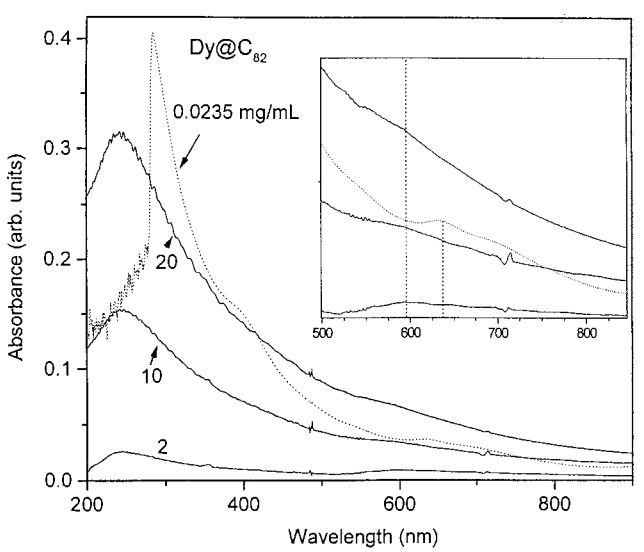

Fig. 5. UV–vis absorption spectra of Dy@C_{82} LB films on quartz plates (solid line) with a different number of deposition steps and Dy@C_{82} dissolved in toluene (dotted line). The inset enlarges the spectral portion of 500–850 nm.

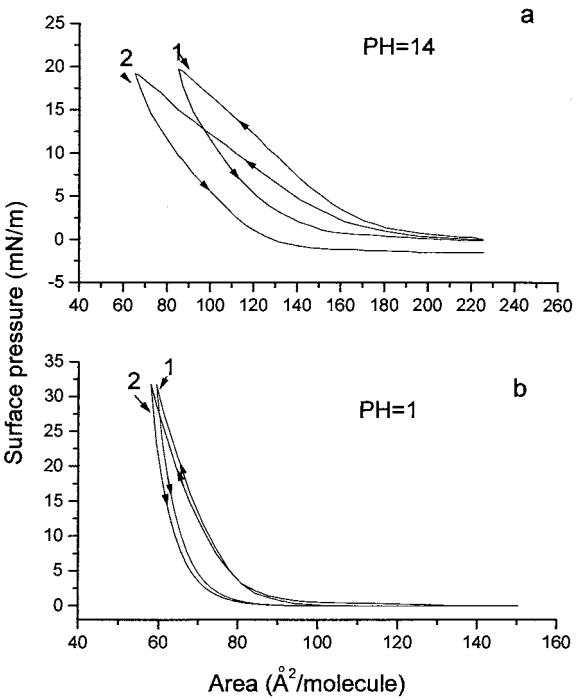

Fig. 6. π–A isotherms of Dy@C_{82} with subphases at pH $\approx$ 14 (a) and pH $\approx$ 1 (b). The isotherms were recorded at a compression–expansion speed of $\sim$1 cm min^{-1}, after two cycles reversed at 20 mN m^{-1}.

subphase pH values of 14 and 1. In particular, the isotherm curves with acidic subphase ($\sim$3.1 mN molecule Å^{-2} for the first cycle in Fig. 6(a)) are much steeper than those with a basic subphase ($\sim$0.9 mN molecule Å^{-2} for the first cycle in Fig. 6(b)). In the process of compression at pH $\approx$ 14, we noticed that the LB trough wall (Teflon tape) was gradually blackened due to the accumulation of the metallofullerenes on the wall above the water surface. This indicates that the metallofullerenes became hydrophobic with the basic subphase. One of the explanations for this is that the metallofullerene balls were somehow broken by a base-catalyzed reaction when a basic solution was used as the subphase. We believe that it is because of the running away of the metallofullerenes from the air–basic water interface, the nominal molecular area of the second cycle becomes much smaller than that of the first cycle at high surface pressure. Furthermore, due to the deposition of metallofullerenes on the Whehely plate for the same reason as described above, the reverse curve 2 could not reach its original location with the expected zero surface pressure. Instead, the surface pressure went negative. This became even more severe in subsequent compression–expansion cycles at pH $\approx$ 14.

The compression–expansion behavior at pH $\approx$ 1 is similar to that at pH $\approx$ 7. This indicates that the metallofullerene cages could survive the breakage at the air–acidic subphase interface. The limiting molecular area observed from the isotherms in Fig. 6(b), however, is more than twice that estimated from Fig. 2. A likely scenario is that under a strong basic condition, the carbon cages may be over oxygenated, resulting ultimately in the destruction of the cages, whereas under acidic conditions, the extent of oxygenation may be moderate without breaking the metallofullerene cages. This is reasonable because metallofullerenes are known to be excellent electron acceptors [17], which would be readily attacked by the HO^- ions under basic conditions. This would facilitate the oxidation of the metallofullerenes. A similar situation is not expected to occur under acidic conditions. The reason why the limiting molecular area at pH $\approx$ 1 is larger than that at pH $\approx$ 7 may indicate that the LB film of Dy@C_{82} is closer to a monolayer regime.

4. Summary and conclusions

For the first time we have successfully constructed multilayer LB films of the endohedral metallofullerene Dy@C_{82} at the air–water surface. Short-range ordered and layered metallofullerene particle assemblies were clearly observed by high-resolution TEM. Blue-shifted UV–vis absorption peaks were identified and attributed to the oxidation of the metallofullerene particles. All the experimental results suggest that the metallofullerenes are intact in the LB films albeit oxygenated. Moreover, oxidation can be minimized by avoiding extended exposure of the metallofullerene LB film to the air. The LB film spreading behavior of Dy@C_{82} was also investigated at different pH values of the water subphase. The basic subphase was found to destroy the metallofullerene cages at the air–water interface, whereas the acidic subphase preserve the integrity of the metallofullerene cages in spite of the inevitable oxidation.

Acknowledgements

This work was supported by a grant from the UGC of Hong Kong.

References

[1] Y.S. Obeng, A.J. Bard, J. Am. Chem. Soc. 113 (1991) 6279.
[2] T. Nakamura, H. Tachibana, M. Yumura, M. Matsumoto, R. Azumi, M. Tanaka, Y. Kawabata, Langmuir 8 (1992) 4.
[3] R. Back, R.B. Lennox, J. Phys. Chem. 96 (1992) 8149.
[4] J. Milliken, D.D. Domonguez, H.H. Nelson, W.R. Barger, Chem. Mater. 4 (1992) 252.
[5] J. Guo, Y. Xu, Y. Li, C. Yang, Y. Yao, D. Zhu, C. Bai, Chem. Phys. Lett. 195 (1992) 625.
[6] L.O. Bulhoes, Y.S. Obeng, A.J. Bard, Chem. Mater. 5 (1993) 110.
[7] Y. Tomioka, M. Ishibashi, H. Kajiyama, Y. Taniguchi, Langmuir 9 (1993) 32.

[8] (a) D. Zhou, L. Gan, C. Luo, H. Tan, C. Huang, G. Yao, X. Zhao, Z. Liu, X. Xia, B. Zhang, J. Phys. Chem. 100 (1996) 3150. (b) D. Zhou, L. Gan, C. Luo, C. Huang, Y. Wu, Solid State Commun. 102 (1997) 891.
[9] D.M. Guldi, Y. Tian, J.F. Fendler, H. Hungerbuhler, K.D. Asmus, J. Phys. Chem. 100 (1996) 2753.
[10] (a) H. Murakami, Y. Watanabe, N. Nakashima, J. Am. Chem. Soc. 118 (1996) 4484. (b) T. Nakanishi, H. Murakami, N. Nakashima, Chem. Lett. (1998) 1219.
[11] D.S. Bethune, R.D. Johnson, J.R. Salem, M.S. de Vries, C.S. Yannoni, Nature 366 (1993) 123.
[12] J.Q. Ding, S.H. Yang, Chem. Mater. 8 (1996) 2824.
[13] J.Q. Ding, L.T. Weng, S.H. Yang, J. Phys. Chem. 100 (1996) 11120. (b) J.Q. Ding, S.H. Yang, Angew. Chem. Int. Ed. Engl. 35 (1996) 2234.
[14] (a) H.J. Huang, S.H. Yang, J. Phys. Chem. B 102 (1998) 10196. (b) G. Gu, H.J. Huang, S.H. Yang, P. Yu, J. Fu, G.K.L. Wong, X. Wan, J. Dong, Y. Du, Chem. Phys. Lett. 289 (1998) 167.
[15] M. Takata, B. Umeda, E. Nishibori, M. Sakata, Y. Saito, M. Ohno, H. Shinohara, Nature 377 (1995) 46.
[16] D.Y. Sun, H.J. Huang, S.H. Yang, Z.Y. Liu, S.Y. Liu, Chem. Mater. 11 (1999) 1003.
[17] H. Shinohara, Endohedral metallofullerenes: structures and electronic properties, in: Advances in Metal and Semiconductor Clusters, vol. 4, JAI Press, Stanford, CT, 1998, pp. 205–226.